De novo sequencing and initial annotation of the Mongolian gerbil (*Meriones unguiculatus*) genome

Diego A.R. Zorio[a,*], Scott Monsma[b], Dan H. Sanes[c], Nace L. Golding[d], Edwin W. Rubel[e], Yuan Wang[a,f,**]

[a] *Department of Biomedical Sciences, College of Medicine, Florida State University, Tallahassee, FL, USA*
[b] *Lucigen Corporation, Middleton, WI, USA*
[c] *Center for Neural Science, New York University, New York, NY, USA*
[d] *University of Texas at Austin, Department of Neuroscience, Center for Learning and Memory, Austin, TX, USA*
[e] *Virginia Merrill Bloedel Hearing Research Center, Department of Otolaryngology-Head and Neck Surgery, University of Washington, Seattle, WA, USA*
[f] *Program in Neuroscience, Florida State University, Tallahassee, FL, USA*

ARTICLE INFO

ABSTRACT

The Mongolian gerbil (*Meriones unguiculatus*) is a member of the rodent family that displays several features not found in mice or rats, including sensory specializations and social patterns more similar to those in humans. These features have made gerbils a valuable animal for research studies of auditory and visual processing, brain development, learning and memory, and neurological disorders. Here, we report the whole gerbil annotated genome sequence, and identify important similarities and differences to the human and mouse genomes. We further analyze the chromosomal structure of eight genes with high relevance for controlling neural signaling and demonstrate a high degree of homology between these genes in mouse and gerbil. This homology increases the likelihood that individual genes can be rapidly identified in gerbil and used for genetic manipulations. The availability of the gerbil genome provides a foundation for advancing our knowledge towards understanding evolution, behavior and neural function in mammals.
Accession number: The Whole Genome Shotgun sequence data from this project has been deposited at DDBJ/ENA/GenBank under the accession NHTI00000000. The version described in this paper is version NHTI01000000. The fragment reads, and mate pair reads have been deposited in the Sequence Read Archive under BioSample accession SAMN06897401.

1. Introduction

The Mongolian gerbil or jird (*Meriones unguiculatus*, Fig. 1A) belongs to the muridae family of rodentia, along with mice and rats, and originated in the steppes of Mongolia [1,2]. The Gerbillinae subfamily includes 14 genera [3], and a DNA sequence analysis of two complete mitochondrial genes suggests a split with lineage leading to mice and rats approximately 13 million years ago [4]. This split is associated with certain specializations that make the gerbil of interest to a broad range of scientists.

Gerbils have many sensory characteristics that make them a favorable species for studies of vision and audition. For example, they are primarily diurnal [5] and possess superior acuity and photopic vision, as compared to mice or rats [6]. Their retinal structure is more analogous to humans, having a relatively high percentage of cone photoreceptors, as compared to mice [7,8]. For this reason, gerbils have been used to study retinal physiology [9,10] and for developing therapeutic drugs and gene delivery approaches following retinal damage [11,12]. Gerbils also display human-like sensitivity to the low sound frequency range that supports speech perception [13,14], whereas mice and rats are more sensitive to very high frequency sounds [15]. Because of this specialization, the gerbil auditory pathway has been intensively studied for its structural and functional specializations, and it serves as a popular model for understanding the neural basis of auditory processing in normal and hearing-impaired animals [16–25]. Examples include middle and inner ear function [26–28], binaural processing in the auditory brainstem [29], parallel information streams of ascending auditory pathway [30–33], auditory perception and integration with other sensory modalities in the primary auditory cortex [18,22], vocal behaviors [34–36] as well as age-dependent hearing loss [37,38].
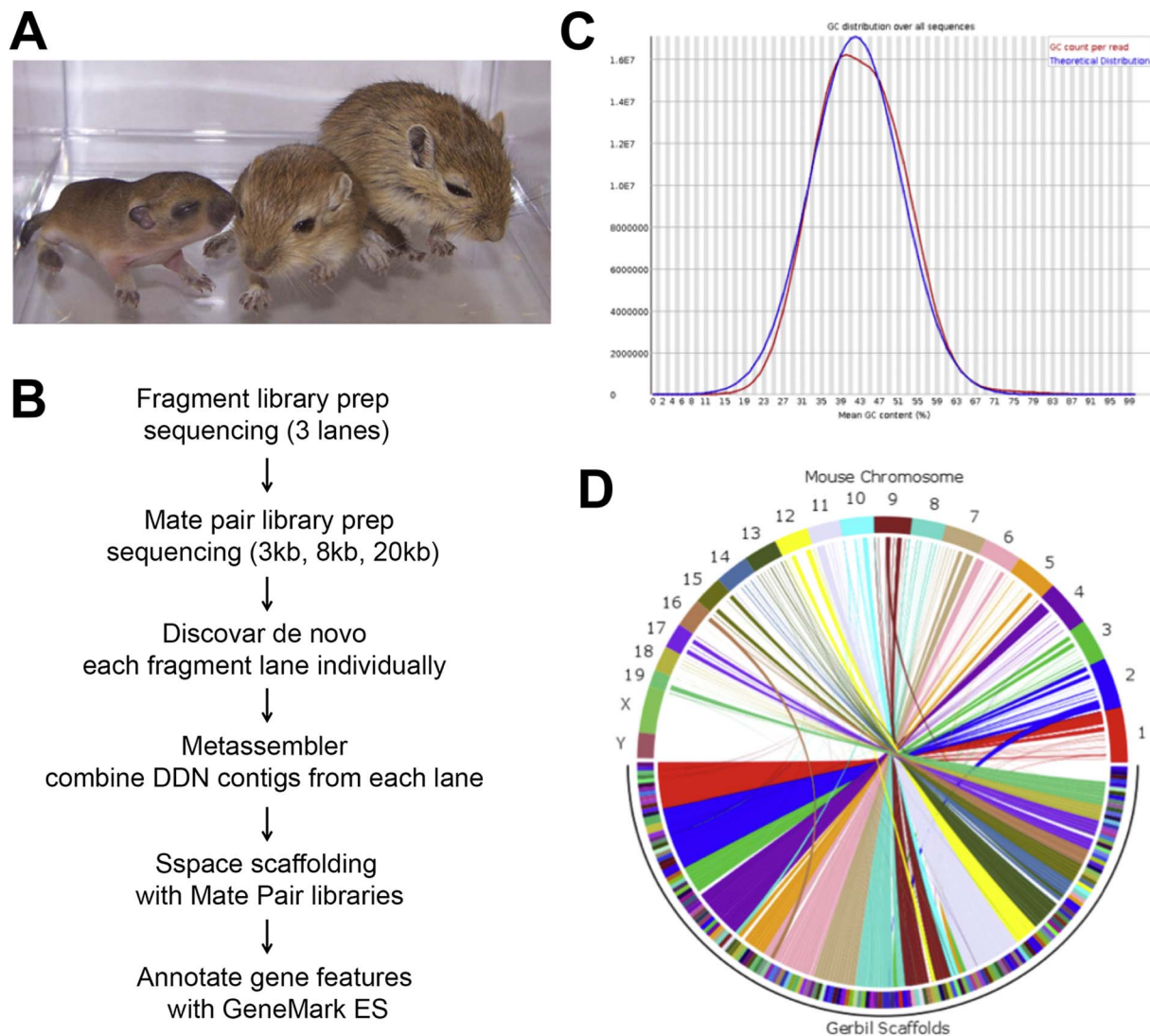
Fig. 1. Gerbil genome assembly. A. Mongolian gerbil (*Meriones unguiculatus*) at ages of postnatal day (P) 9, 16 and 21 from left to right. Scale bar is 10 cm. B. Workflow of genome assembly. C. GC content of Mongolian Gerbil genome, determined from fragment library reads using FastQC. The distribution shows a slightly skewed shape and is consistent with the overall assembly GC content of 42.09%. D. Synteny map of Mouse GRCm38 chromosomes versus 1 Mbp scaffolds of Gerbil assembly. In the circle diagram, gerbil scaffolds (bottom half) are reordered according to syntenic matches with the mouse chromosomes (top half). No syntenic blocks are observed for the mouse Y chromosome, and very little for the mouse X chromosome. Blocks corresponding to scaffolds with potential translocations are also evident as off-center arcs: blue from mouse chromosome 2; brown from mouse chromosome 9, yellow from mouse chromosome 12 and tan from mouse chromosome 16. (For interpretation of the references to colour in this figure legend, the reader is referred to the web version of this article.)

Gerbils are well suited to study a range of pathological conditions, including epilepsy (seizures) and cerebral ischemia (stroke). Gerbils are known to have high susceptibility to seizures that can be induced by simple external stimuli [39,40]. Studies in gerbils have identified abnormal GABAergic dependent synaptic transmission as an important underlying mechanism of seizures [41–43]. Investigations using gerbils as a stroke model have shown that "stroke-prone" and "stroke-resistant" gerbils are associated with the conditions of posterior communicating arteries in the circle of Willis [44–48]. In addition, the gerbil has been commonly used for studying a number of parasitic, viral and bacterial diseases (reviewed in [2]). For example, humans have benefitted with the development of serologic tests and treatment regimens against lymphatic filariasis by studying gerbils infected with filarid nematodes [49–50]. Gerbils are also used to study gastric ulcers caused by Helicobacter pylori infections as they develop severe gastritis and ulcers [51].

To advance these and other research areas where the gerbil serves as an appropriate animal model, the whole gerbil genome is needed in order to enable further advances at the genetic and molecular levels.

We report the whole gerbil genome sequence and initial annotation, providing a fundamental database for gene analyses as well as the development of genetic editing approaches. We compare the gerbil genome to the human and mouse genomes, with the goal of identifying both important similarities and differences across species. As a first application of this gerbil genome database, we also analyzed the chromosomal structure of eight individual genes that are extensively studied in mammalian neural signaling and demonstrate the possibility of further studying these genes at previously unachieved levels.

2. Material and methods

2.1. Animals and tissue preparation

Mongolian gerbils (*Meriones unguiculatus*), strain 243, were purchased from the Charles River Laboratories (Wilmington, MA). One male animal of 6 weeks of age was used for tissue extraction for this project. All procedures were approved by the Florida State University Institutional Animal Care and Use Committee and conformed to NIH

guidelines. Tissues from leg muscle were extracted, immediately flash frozen in liquid nitrogen and stored at −80 °C until further processing.

2.2. DNA extraction

For high molecular-weight genomic DNA extraction, leg muscle tissue was thawed and minced finely with a razor blade, then refrozen on dry ice and ground to fine powder with liquid nitrogen. Powdered tissue (1–2 g) was resuspended in 600 μl gDNA extraction buffer (60 mM Trisaminomethane hydrochloride (Tris-HCl) pH 8.0, 100 mM Ethylenediaminetetraacetic acid (EDTA), 0.5% SDS) plus 50 μl Proteinase K (800 U/ml, New England Biolabs) and incubated at 50 °C for 3 h followed by 37 °C overnight. Debris were removed by centrifugation and the supernatant was extracted with phenol followed by chloroform:isoamyl alcohol (96:4). The recovered aqueous phase was treated with RNase cocktail for 30 min at 37 °C, and the DNA was precipitated by the addition of 1:10 volume sodium acetate (3 M, pH 5.0) and two volumes of isopropanol. DNA pellets were washed with 70% ethanol and resuspended in 100 μl elution buffer (10 mM Tris, 0.5 mM EDTA). Genomic DNA was quantified using Qubit High Sensitivity reagents.

2.3. Library construction, sequencing and assembly

Genomic DNA was ultrasonically sheared to 300 base pairs (bp) in micro-TUBE strips (Covaris, LE220 instrument) for fragment libraries. For mate pair libraries, DNA was sheared to 3-, 8- and 20-kilo bases (kb) using Covaris gTubes. Fragment libraries were constructed with the NxSeq AmpFree kit (Lucigen), and mate pair libraries with the NxSeq Long Mate Pair kit (Lucigen) following manufacturers' instructions. Fragment libraries were sequenced on three lanes of HiSeq X (Illumina) with 2 × 150 paired end (PE) chemistry at the Hudson Alpha Institute for Biotechnology (Huntsville, AL). Mate pair libraries were sequenced on MiSeq (Illumina) 2 × 150 PE with V2 chemistry. Mate pair data was processed with Python scripts Illumina-Chimera-Clean5.py and IlluminaJunctionSplit9.py (available from Lucigen) to remove chimeric mate pairs and to trim the right and left mates by detection of the Junction Code sequence.

Initial assembly was performed with Discovar De Novo (ftp://ftp.broadinstitute.org/pub/crd/DiscovarDeNovo/latest_source:code/LATEST_VERSION.tar.gz; Accessed 4 November 2016.) using untrimmed fragment data as suggested in the Discovar manual. Each lane of HiSeq X data was assembled individually. The three sets of final Discovar De Novo contigs were then merged into a single assembly by using Metassembler v1.5. [https://sourceforge.net/projects/metassembler/files/latest/download] [52]. Metassembler contigs were then scaffolded sequentially with the 3-, 8- and 20-kb mate pair libraries using a stand-alone scaffolder of pre-assembled contigs using paired-read data (SSPACE) Basic v2.0 [https://www.baseclear.com/services/bioinformatics/basetools/sspace-standard/] [53]. Repetitive sequences were identified by using Repeat Modeler v1.08 [http://www.repeatmasker.org/RepeatModeler/] ([54]; Accessed 7 March 2017) for de novo repeat discovery. The unmasked assembly was filtered to remove all contigs smaller than 1 kb following the National Center for Biotechnology Information (NCBI) Eukaryotic Genome Annotation Pipeline guidelines ([55]; Accessed 17 May 2017) and the remainder was deposited with GenBank and submitted for annotation by the NCBI Eukaryotic Genome Annotation Pipeline [https://www.ncbi.nlm.nih.gov/genome/annotation_euk/].

Syntenic blocks between mouse GRCm38 chromosomes and gerbil scaffolds were identified using Symap 4.2 [http://www.agcol.arizona.edu/software/symap/v4.2/download] [56], after filtering the gerbil assembly for scaffolds of over 1 mega base pairs (Mbp) (658 scaffolds total). Orthologous gene groups were identified between the Gerbil protein set, the human proteome (UP00005640_9606) and the mouse proteome (UP00000589_10090) from UniProt [http://www.uniprot.

org/downloads; Accessed 20 April 2017]. The TriFusion v0.5.0 pipeline [https://pypi.python.org/pypi/trifusion/0.5.0.post3; Accessed 7 April 2017] [57], which incorporates Usearch for protein-protein comparisons and the OrthoMCL pipeline [58], was used for proteome comparisons and generation of orthologous protein families. Gene functional annotation clustering was performed with DAVID 6.8 [https://david.ncifcrf.gov; Accessed 24 April 2017] [59] using 194 human Uniprot accession numbers for unique orthologs shared between human and gerbil. The mouse Uniprot accession numbers were used for 760 unique orthologs shared between mouse and gerbil, and for 538 unique orthologs shared between mouse and human (Supplementary file "multi-list.txt").

3. Results and discussion

3.1. Gerbil genome assembly

Genomic DNA extracted from leg muscle tissue of an adult male *Meriones unguiculates* of 6 weeks of age was used to construct fragment and mate pair libraries for sequencing on the Illumina platform, following the work flow shown in Fig. 1B. Fragment libraries were sequenced on 3 lanes of HiSeqX, generating 407.4 Gigabases (Gbases) of raw data (163 × genomic coverage based on a genome size of 2.5 Gbases). Unfiltered reads from each lane were assembled with Discovar De Novo to generate 3 initial assemblies that were merged into a single assembly with Metassembler. The merged assembly was then scaffolded sequentially with multiple mate pair libraries (3, 8 and 20 kb insert size) using SSPACE. The final assembly was filtered for contigs and scaffolds ≥1 kb resulting in 68,793 scaffolds with N50 of 374,687 bp and a total length of 2.523 Gbp (Table. 1). This corresponds to 98.1% of the size of the current reference mouse genome (GRCm38.p4) of 2.671 Gbp. The average GC content (the percent of guanine and cytosine bases present on the DNA) of the gerbil assembly was 42.09% (Fig. 1C), similar to the mouse at 42.49%.

Repeats were identified de novo using RepeatModeler, resulting in masking of 33.82% of the genome (853 megabases (Mbases) in 3.8 million elements) (Table S1). These repeats were mainly consisting of LINE1 type elements (13.48% of genome) and unclassified elements (15.78% of genome) with a smaller contribution of LTR elements (1.54% of genome). For comparison, the NCBI annotation masked 35.94% of the genome with RepeatMasker and 30.74% with WindowMasker. The genome masked with WindowMasker was used for subsequent alignment of transcripts and proteins during the NCBI annotation run. The relatively low percentage (34%) of the gerbil genome as repetitive sequences, as compared to the mouse reference genome (44.16%), is likely due to known difficulties with assembly of repetitive sequences leading to the exclusion of small contigs and highly repetitive regions from the draft assembly [64]. Further improvement of the gerbil assembly will allow more detailed analysis by resolving these

Table 1
Summary of assembly statistics showing number of contigs/scaffolds, N50, NG50 and % GC content. The assembly was filtered for compliance with NCBI annotation guidelines. Scaffolds and unplaced contigs of < 1 kb length were filtered, which removed 316,114 short contig/scaffolds (average length 309 bp) accounting for 3.7% of the initial assembly length (97.7 Mbp).

Total contigs/scaffolds	384,902
Total bp	2,620,810,971
Scaffolds/contigs ≥1 kb	68,788
Total bp ≥ 1 kb	2,523,112,562
	(96.3% of total bp)
(excluding Ns)	2,402,558,981
	(4.77% gaps = N)
Scaffold N50	351,937 bp
Scaffold L50	13,038
Maximum scaffold	6,569,692 bp
GC content	42.09%

Table 2

De novo gene annotations. Annotations were generated by the NCBI eukaryotic annotation pipeline, using existing gerbil transcripts, proteins, and RNA-Seq data from the Sequence Read Archive (SRA) as evidence.

	NCBI annotation	Mean length (bp)	Median length (bp)	Minimal length (bp)	Maximum length (bp)
start_codon	38,750				
Exon	227,097	262	135	1	17,106
Intron	201,876	3803	1312	30	452,462
CDS	38,750	1809			
All transcripts	40,519	2708	2212	55	99,751
mRNA	59,721	2774	2266	117	99,751
misc_RNA	487	2678	2449	211	10,553
tRNA	396	74	72	69	84
lncRNA	886	995	648	55	8241
Gene	23,273	31,095	14,417	69	753,783

Table 3

Synteny mapping against mouse GRCm38 reference genome. 658 gerbil scaffolds of length > 1 Mpb were mapped against the reference mouse chromosomes, and the relative coverage of the mouse chromosomes is indicated (% Mouse Covered) along with count of syntenic blocks found (#Synteny blocks). A total of 346 syntenic blocks were detected.

Mouse chromosome	Mouse chr length	% Mouse covered	% Double coverage	# Synteny blocks
1	195,472,000	25%	2%	56
2	182,113,000	30%	1%	58
3	160,039,000	24%	0%	44
4	156,508,000	30%	2%	40
5	151,834,000	25%	1%	43
6	149,736,000	32%	1%	63
7	145,441,000	27%	0%	54
8	129,401,000	35%	1%	48
9	124,595,000	30%	0%	43
10	130,695,000	19%	2%	44
11	122,082,000	43%	1%	56
12	120,129,000	27%	0%	38
13	120,421,000	26%	2%	44
14	124,902,000	20%	0%	33
15	104,043,000	20%	1%	26
16	98,207,000	14%	1%	31
17	94,987,000	30%	2%	33
18	90,702,000	20%	2%	25
19	61,431,000	36%	0%	22
X	171,031,000	2%	0%	12
Y	91,744,000	0%	0%	0

differences with long read sequencing approach [65].

The masked genome was annotated by the NCBI pipeline mainly by alignment of transcripts, proteins, and existing Gerbil RNA-Seq data from the Sequence Read Archive (SRA) from NCBI. A total of 38,750 mRNAs composed of 227,097 exons were annotated for a total of 23,273 genes (Table 2). Completeness of the assembly was assessed by comparing the 38,750 encoded proteins to the Euarchontoglire single copy orthologous protein database (6192 sequences) with Benchmarking Universal Single-Copy Orthologs (BUSCO) [60] (Table S2). This analysis found 93.6% complete Buscos with 40.1% duplicated. An additional 4.9% of Buscos found were fragmented, and 1.5% were missing.

Since this is the first report on genome assembly and annotation of the gerbil genome we compared it with other short assembled genomes from other close related species. The assembly metrics (contig N50 of 46.5 kb; annotated protein count 38,763; total length 2523 Mb and GC content 42.1%) are comparable to other short read-based Muroidea de novo genome assemblies such as *Cricetulus griseus* (Chinese hamster, https://www.ncbi.nlm.nih.gov/assembly/GCF_000223135.1. Accessed 20 Feb 2018) and *Peromyscus maniculatus* (prairie deer mouse, https://www.ncbi.nlm.nih.gov/assembly/GCF_000500345.1. Accessed 20 Feb 2018).

Further analysis revealed not surprisingly, that the majority of identified gerbil genes (81%) are shared between mouse and human. Similarly, it has been found that the complete mitochondrial genome sequence of *M. unguiculatus* (GenBank accession nos. KF425526 and NC_023263) displays the typical complement of 37 genes, and a similar base composition and codon usage as compared to several other rodent species [61,62] Almost identical sequence of gene and protein for 8 individual genes further indicate that these shared genes are highly conserved among these species. For the remaining 19% of genes, 6% are shared between gerbil and mouse, while only 1.5% are shared with human. This observation is not surprising as gerbils and mice belong to the muridae family of rodentia and are far closer evolutionarily than gerbils and humans. Interestingly, the genes shared only between human and gerbil, appear to be mainly involved in gene expression and gene regulation, while the genes shared only by mouse and gerbil are dominated by olfactory and gustatory sensing. Although a more detailed analysis of the particular gene regulatory networks shared by human and gerbil is needed to understand the basis of these differences, one plausible explanation could be shared characteristics of social structure such as communal living.

3.2. Comparison to mouse genome

Meriones unguiculatus belongs to the Muridae family, which includes mouse and rat. The gerbil karyotype, like the rat, contains 21 chromosomes compared to 20 for the mouse [63]. We examined synteny with the mouse genome by mapping gerbil scaffolds of over 1 Mbp length (683 scaffolds totaling 556 Mbp, equal to 22% of the draft gerbil genome; Fig. 1D; Table 3). Overall, 346 syntenic blocks were found among the mouse autosomes, amounting to 27% coverage of the mouse genome with 1% doubled coverage. Syntenic blocks corresponding to scaffolds with translocations were evident for mouse chromosomes 2, 12 and 16. Coverage of the mouse autosomes varied between 14% (chromosome 16) to 43% (chromosome 11). Only 2% of the mouse X chromosome was covered in 12 syntenic blocks, and no syntenic regions were found on the mouse Y chromosome. This low percentage of syntenic blocks between mouse chromosomes and gerbil scaffolds is not unexpected given divergence of *Gerbillidae* sex chromosomes and apparently autosomal translocations into the X and Y chromosomes [66–69].

3.3. Comparison to mouse and human proteomes

The 38,750 gerbil proteins encoded by the consensus gene set were compared to the human and mouse reference proteomes (GRCh38 and GRCm38 from UniProt) using TriFusion to determine orthologous groups. From a total dataset of 1,728,973 protein sequences for all three species, 19,395 total orthologs were detected as shown in Fig. 2 as numbers inside Venn diagram. These numbers include 11,225 single-copy orthologs. 81.3% of the total orthologs were shared between all three taxa (15,773 total), while 84.7% were shared only between human and mouse (16,426 total). Gerbil shared 87.2% with mouse (16,911 total) and 82.8% with human (16,058). 1029 of orthologs were unique to gerbil, compared to 281 and 236 unique to mice and human respectively. The 1029 ortholog groups unique to gerbil contained a total of 2652 annotated protein sequences, and 734 of the ortholog groups (71%) contained only 2 members with the remainder containing 3 to 12 members. The majority of the 1029 gerbil ortholog groups were attributable to annotated protein isoforms (780, 76%).

DAVID analysis of functional annotation enrichment for 760 genes shared by gerbil and mouse but not human resulted in 60 enriched clusters, with the highest cluster enrichment score of 71.71 (DAVID enrichment score equals the geometric mean of the annotation term's modified Fisher Exact p-values expressed as -log [https://david.ncifcrf.gov/helps/functional_annotation.html#fisher]) for the cluster

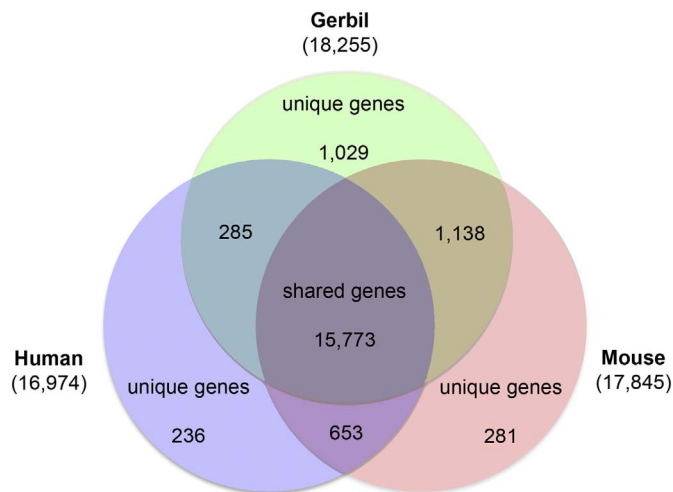**Fig. 2.** Common genes shared among human, mouse and Mongolian gerbil. The 38,750 protein sequences of gerbil annotated by the NCBI pipeline were compared to the mouse and human reference proteomes (GRCh38 and GRCm38) to identify orthologs. A total of 19,395 ortholog groups were identified, the majority of which are shared by all three species (15,773; 81.3%). Gerbil shared 87.2% with mouse (16,911 total) and 82.8% with human (16,058), while 84.7% were shared only between human and mouse (16,426 total). 1029 ortholog groups were unique to gerbil (5.3%), compared to 281 unique to mouse and 236 unique human ortholog groups. The majority of the 1029 gerbil ortholog groups were attributable to annotated protein isoforms (780, 76%).

containing GO terms "sensory perception of smell" (6.1-fold enrichment, p-value 7.61e−115) and "olfactory receptor activity" (5.5-fold enrichment, p-value 2.19e−107). The next highest cluster had an enrichment score of 3.60 and contained GO terms "response to stimulus" (3.9-fold enrichment, p-value 1.18e−8) and "bitter taste receptor activity" (8.2-fold enrichment, p-value 9.12e−6). In contrast, analysis of 194 genes shared by gerbil and human but not mouse resulted in 25 enriched term clusters with enrichment scores of < 2, with the highest enrichment score of 1.69 for the cluster containing GO term "RNA binding" (2.9-fold enrichment, p-value 9.99e−4) followed by a cluster with enrichment score of 1.52 containing GO term "sequence specific DNA binding" (2.4-fold enrichment, p-value 1.5e−2). Mouse-human shared gene analysis (538 genes) yielded 76 enriched clusters with maximum enrichment score of 2.9 for the cluster containing for GO term "synapse" (2.7-fold enrichment, p-value 1.50e−4), enrichment score 2.9 for the cluster containing GO term "GTP-binding" (3.5-fold enrichment, p-value 7.34e−7), and enrichment score 2.49 for the cluster containing GO term "ion transport" (which includes neurotransmitter-gated ion channels and extracellular ligand-gated ion channels; 12.4-fold enrichment, p-value 9.77e−5). Blastp [70] and ProSplign [https://www.ncbi.nlm.nih.gov/sutils/static/prosplign/prosplign.html] [71]. (Accessed 22 Feb 2018) alignments against human and mouse RefSeq proteomes yielded average protein sequence identity of 73.2 and 76.03% respectively, and average query alignment of 80.25 and 84.55% respectively (Table S3).

The annotated gerbil protein sequences were classified into the Kyoto Encyclopedia of Genes and Genomes (KEGG) functional categories using Ghost-Koala [GhostKoala [http://www.kegg.jp/ghostkoala/]. Accessed 27 April 2017] and compared to the mouse and human reference protein sets (Fig. 3). A total of 70.1% (27,182 out of 38,750) gerbil proteins were assigned to KEGG categories. The top two categories were *Human Diseases* (5755 hits) and *Organismal Systems* (4596 hits), similar to human and mouse. *Metabolism* and *Environmental Information Processing* were next (3664 hits and 3389 hits, respectively), followed by *Cellular Processes* (2065 hits) and *Genetic Information Processing* (1195 hits). Altogether these top six categories accounted for 20,664 (76%) of the 27,182 proteins assigned.
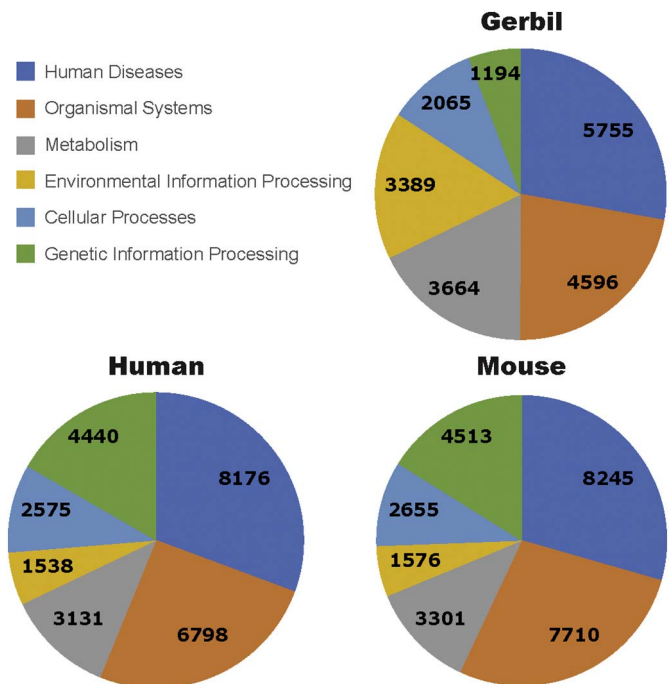

Fig. 3. Venn diagram comparing protein functional assignments among human, mouse and Mongolian gerbil. Protein sequences of gerbil were annotated by the NCBI pipeline were assigned to KEGG orthology groups and functional category counts were compared to the mouse and human references. As seen in the pie charts, the two largest categories for all three species are Human Diseases and Organismal Systems. Gerbil however, has a larger number of hits under the Environmental Information Processing and Metabolism categories when compared to humans and mouse. In contrast, gerbil shows relatively fewer hits in Genetic Information Processing. Numbers in the pie chart show the actual number of hits represented in GO terms in each category for that species.

3.4. Detailed comparison to eight mouse genes

To refine the comparison to known mouse genes at a finer level, we searched the assembly for scaffolds corresponding to 8 specific genes with great interests in the field of sensory processing and social interaction; two areas where gerbil physiology and behavior resemble human characteristics more closely than mice characteristics. These 8 genes can be divided into two groups. Genes in the first group (*ATP2B2*, *Gabra1*, *Gabrb2*, *Kcna1*, *Kcnc1* and *Gphn*) have important function in regulating neuronal activity and some are particularly critical for the survival and normal function of fast-spiking auditory cells and neurons. The gene *ATP2B2* encodes the type 2 of the plasma membrane calcium ATPase (PMCA2). PMCA is a major calcium efflux system that sets the resting calcium concentration [72–74]. PMCA2, the most efficient type of PMCA, is necessary for hair cell survival in the cochlea. Spontaneous and induced mutations in *ATP2B2* are associated with hearing loss in both humans and mice [75–82]. In addition, PMCA2 is highly expressed in auditory neurons and is involved in the tonotopic organization of auditory cell groups [83,84]. *Gabra1* and *Gabrb2* encode the two essential subunits, alpha 1 and beta 2, of GABA receptors that underlie the chief inhibitory neurotransmission in the brain. In mice and human, *Gabra1* and *Gabrb2* mutations have been associated with generalized and syndromic epilepsy as well as with intellectual disabilities [85–87]. Gephyrin, encoded by *Gphn*, is a neuronal assembly protein that anchors inhibitory neurotransmitter receptors, including GABA receptors, to the postsynaptic cytoskeleton [88]. *Kcna1* and *Kcnc1* are the genes for voltage-gated potassium channels Kv1.1 and Kv3.1, respectively. These two potassium channels are necessary and kinetically optimized for high-frequency action potential generation and temporal processing with submillisecond temporal resolution [89–91]. The availability of the gerbil genome enables genetic approaches for further determining the roles of these genes in the gerbil, an advantageous model for
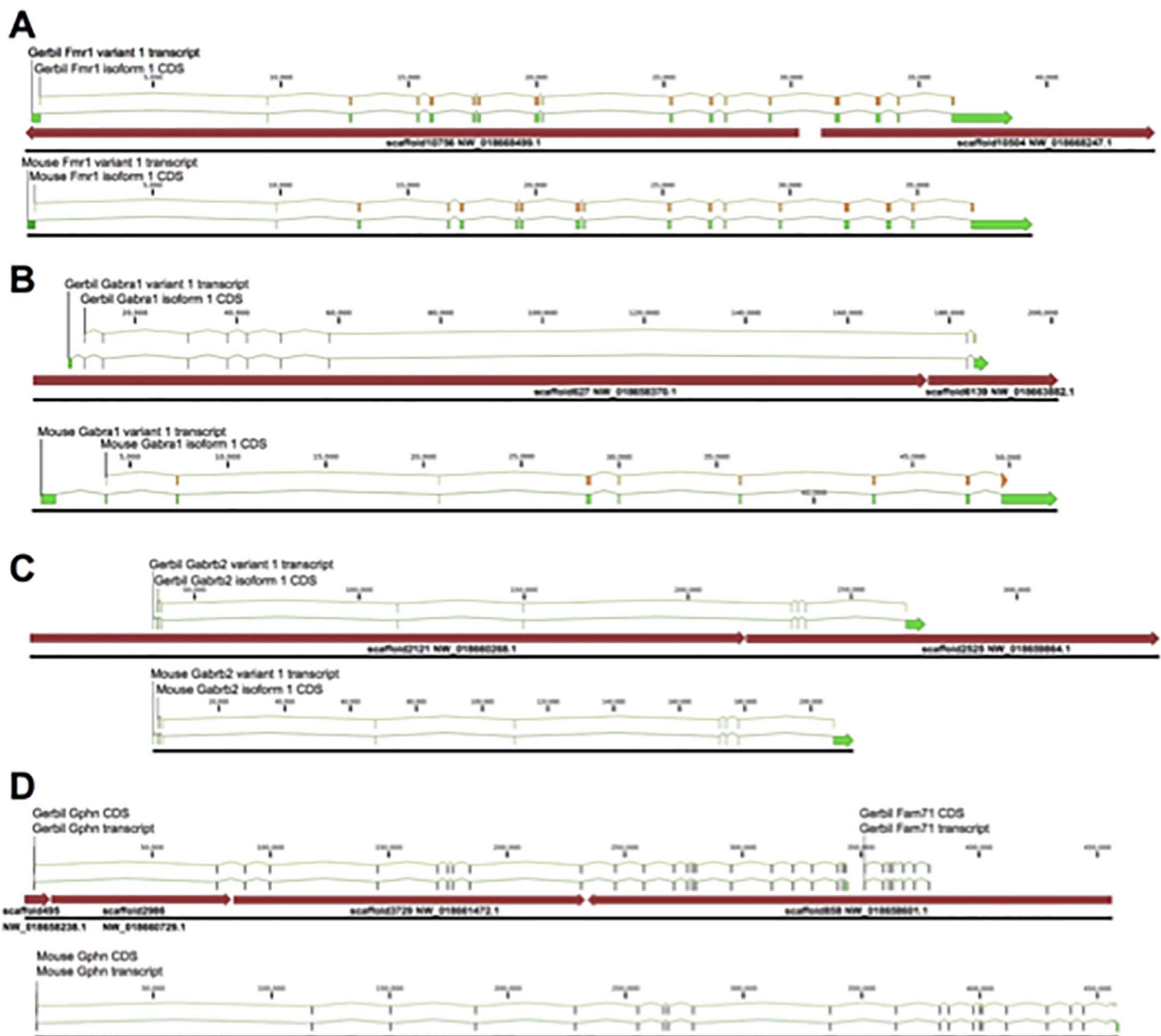
Fig. 4. Comparative gene structure for 8 orthologs between gerbil and mouse. The mouse gene and mRNA sequences (green) were used to identify homologous Mongolian gerbil scaffolds (brown arrows) using blast. Comparison at the nucleotide level enabled identification of splice junctions and protein coding sequences (CDSs, illustrated in orange), due to the high level of relatedness between the two species. A, Fragile X-mental retardation gene (FMR1). B, Gamma amino butyric acid receptor alpha 1 gene (Gabra1). Note that mouse and gerbil genes are drawn to different scales due to large size of the penultimate intron in the gerbil Gabra1 gene. However, the significance of the apparent intron enlargement is unclear and could be attributable to the de novo assembly artifacts. C, Gamma amino butyric acid receptor beta 2 gene (Gabrb2). D, Gephyrin gene (Gphn). A flanking Fam71 gene is downstream of the Gphn gene in both gerbil (showing here) and mouse (not illustrated). E, Potassium voltage-gated channel subfamily a member 1 (Kcna1). F, Oxytocyn receptor (Oxtr). G, Potassium voltage-gated channel subfamily C member 1 (Kcnc1). H, ATPase plasma membrane Ca^{2+} transporting 2 (PMCA2). (For interpretation of the references to colour in this figure legend, the reader is referred to the web version of this article.)

studying hearing, especially with regard to temporal processing and for studying epilepsy.

The second group contains *Fmr1* and *Oxtr*, two genes extensively involved in neurological disorders associated with communication and social deficits. Transcriptional silencing of *Fmr1* and the resultant loss of its product, the fragile x mental retardation protein (FMRP), are responsible for the fragile X syndrome (FXS) [92,93]. FXS is characterized with prominent auditory dysfunction and autism-like social difficulties. Examination of human FXS and/or autism brains reveal dramatically disorganized auditory brainstem in particular the medial superior olive (MSO), a center for auditory temporal processing [94–98]. Gerbils, but not mice, display a well-developed MSO that is structurally and functionally comparable to human [99]. An FMRP knockout gerbil strain can serve as a disease model for FXS and help

determine the pathology of auditory dysfunction especially those associated with temporal processing.

The oxytocin receptor (OXTR) is a G-protein coupled receptor for the hormone and neurotransmitter oxytocin [100]. Oxytocin receptors are expressed by the myoepithelial cells of the mammary gland, playing an important role as an inducer of uterine contractions during parturition and of milk ejection. Oxytocin receptors are also present in the central nervous system, modulating a variety of behaviors, including stress and anxiety, social memory and recognition, sexual and aggressive behaviors, bonding (affiliation) and maternal behavior [101–104]. The prominent bonding and maternal behaviors in gerbils provide an excellent model for studying OXTR mediated social interactions at the genetic and molecular levels.

Blastn searches using the full mouse gene loci and their major

Fig. 4. (*continued*)

Table 4

Gene structure comparison of 8 genes between gerbil and mouse. Overall, the gerbil genes exhibited extremely similar structure in comparison to mouse. No differences in Exon (E) count were detected, although minor differences in average E length were apparent in all genes except PMCA2. Major differences were seen in average Intron (I) length in Gabra1 and Gpnh, however the significance of the apparent intron expansion is unclear and may be attributable to assembly artifacts. G, Gerbil; M, mouse; Avg., Average; bp, base pairs; ID, Identity.

	Fmr1		Gabra1		Gabrb2		Gpnh		Kcna1		Oxtr		Kcnc1		PMCA2	
Species	G	M	G	M	G	M	G	M	G	M	G	M	G	M	G	M
Exon count	17	17	10	10	10	10	23	23	2	2	2	2	4	4	22	22
Avg. E length (bp)	260	258	749	754	142	143	142	143	4463	4484	2280	2283	1060	1083	195	195
Intron count	16	16	9	9	9	9	22	22	1	1	1	1	3	3	21	21
Avg. I length (bp)	2235	2190	19,563	5257	25,259	22,810	15,509	2068	376	370	12,960	11,558	12,354	12,635	24,419	25,019
Amino acids	615	614	455	455	474	474	772	772	495	495	387	388	585	585	1198	1198
ID	599/615		454/455		474/474		766/772		494/495		370/388		583/585		1194/1198	
	(97.40%)		(99.78%)		(100%)		(99.22%)		(99.80%)		(97.37%)		(99.66%)		(99.67%)	

transcripts allowed identification of 2 to 8 scaffolds covering the entire coding regions of each of the eight genes (Fig. 4). Gerbil exons and CDSs of the major transcript for each gene were annotated by direct genomic sequence comparison of gerbil to mouse. The overall structure of the 8

gerbil genes is nearly identical to that in mouse, with complete conservation of exon counts and specific splice junctions. Minor variation was seen in average exon length, with the most variation occurring in intronic regions. Comparison of the encoded proteins showed 100%

identity for *Gabrb2*, and only 1 to 4 amino acid differences (99.7%–99.8% identity) for *Gabra1, Kcna1, Kcnc1* and *ATP2B2*. *Gphn, Fmr1,* and *Oxtr* were also highly conserved with 6 (99.22% identity), 16 (97.40%) and 18 (97.37%) amino acid differences from mouse proteins, respectively (Table 4). Four of the eight genes were assembled as single scaffolds (*Kcna1, Oxtr, Kcnc1* and *ATP2B2*), while *Fmr1, Gabra1* and *Gabrb2* each spanned two scaffolds. The *Gphn* gene has exons found on four individual scaffolds. Inter-scaffold breaks always occurred within introns, typically in highly repetitive di- or tri-nucleotide repeats.

In summary we have sequenced the *Meriones unguiculatus* genome and reported here its initial sequence annotation and characterization. We have compared our data set with human and mouse genomes. As expected we have found some similarities and some differences among these data sets. We specifically compared the chromosomal structure of eight genes with high relevance for controlling neural signaling and demonstrate a high degree of homology between these genes in mouse and gerbil. Taken together, the information generated in this study provides an extreme valuable resource that will help researchers advance our knowledge in realms of both behavior and neural function at the molecular level.

Author contributions

Conceived and designed the experiments: YW, DARZ, EWR, DS, NG. Contributed Materials: DARZ, YW. Performed the experiments: SM, DARZ. Analyzed the data: SM, DARZ. Wrote the paper: YW, DARZ, SM, DA, NG, EWR.

Conflict of interests

The authors declare no conflict of interests.

Acknowledgements

References

[1] V. Schwentker, The gerbil. A new laboratory animal. Illinois, Veterinarian 6 (1963) 5–9.
[2] M. Batchelder, L.S. Keller, M.B. Sauer, W.L. West, The Laboratory Rabbit, Guinea Pig, Hamster, and Other Rodents, vol. 52, Academic Press, 2012, pp. 1132–1155.
[3] R.M. Nowak, Walker's Mammals of the World, Volume II, Sixth Ed., The John Hopkins University Press, London and Baltimore, 1999.
[4] P. Chevret, G. Dobigny, Systematics and evolution of the subfamily Gerbillinae (Mammalia, Rodentia, Muridae), Mol. Phylogenet. Evol. 35 (3) (2005) 674–688.
[5] S. Yang, X. Luo, G. Xiong, K.F. So, H. Yang, Y. Xu, The electroretinogram of Mongolian gerbil (Meriones unguiculatus): comparison to mouse, Neurosci. Lett. 589 (2015) 7–12.
[6] A.G. Baker, V.F. Emerson, Grating acuity of the Mongolian gerbil (Meriones unguiculatus), Behav. Brain Res. 8 (2) (1983) 195–209.
[7] V.I. Govardovskii, P. Röhlich, A. Szél, T.V. Khokhlova, Cones in the retina of the Mongolian gerbil, Meriones unguiculatus: an immunocytochemical and electrophysiological study, Vis. Res. 32 (1992) 19–27.
[8] A.H. Bytyqi, P.G. Layer, Lamina formation in the Mongolian gerbil retina (Meriones unguiculatus), Anat. Embryol. (Berl.) 209 (2005) 217–225.
[9] T. Zhang, L. Huang, L. Zhang, M. Tan, M. Pu, G.E. Pickard, K.F. So, C. Ren, ON and OFF retinal ganglion cells differentially regulate serotonergic and GABAergic activity in the dorsal raphe nucleus, Sci. Rep. 6 (2016) 26060.
[10] C. Garbers, J. Henke, C. Leibold, T. Wachtler, K. Thurley, Contextual processing of brightness and color in Mongolian gerbils, J. Vis. 15 (1) (2015) 15.1.13.
[11] B. Delbarre, G. Delbarre, C. Rochat, F. Calinon, Effect of piribedil, a D-2 dopaminergic agonist, on dopamine, amino acids, and free radicals in gerbil brain after cerebral ischemia, Mol. Chem. Neuropathol. 26 (1) (1995) 43–52.
[12] M.C. Mauck, K. Mancuso, J.A. Kuchenbecker, T.B. Connor, W.W. Hauswirth, J. Neitz, M. Neitz, Longitudinal evaluation of expression of virally delivered transgenes in gerbil cone photoreceptors, Vis. Neurosci. 25 (3) (2008) 273–282.
[13] D.M. Lay, The anatomy, physiology, functional significance and evolution of specialized hearing organs of gerbilline rodents, J. Morphol. 138 (1) (1972) 41–120.
[14] A. Ryan, Hearing sensitivity of the Mongolian gerbil, Meriones unguiculatis, J. Acoust. Soc. Am. 59 (5) (1976) 1222–1226.
[15] R.S. Heffner, G. Koay, H.E. Heffner, Audiograms of five species of rodents: implications for the evolution of hearing and the perception of pitch, Hear. Res. 157 (1–2) (2001) 138–152.
[16] O. Gleich, J. Strutz, The Mongolian gerbil as a model for the analysis of peripheral and central age-dependent hearing loss, in: Sadaf Naz (Ed.), Hearing Loss, 2012, pp. 67–92 (ISBN: 978-953-51-0366-0; Chapter 4).
[17] L.A. Belliveau, D.R. Lyamzin, N.A. Lesica, The neural representation of interaural time differences in gerbils is transformed from midbrain to cortex, J. Neurosci. 34 (50) (2014) 16796–16808.
[18] E. Budinger, H. Scheich, Anatomical connections suitable for the direct processing of neuronal information of different modalities via the rodent primary auditory cortex, Hear. Res. 258 (1–2) (2009) 16–27.
[19] Y. Wang, H. Sakano, K. Beebe, M.R. Brown, R. de Laat, M. Bothwell, R.J. Kulesza Jr., E.W. Rubel, Intense and specialized dendritic localization of the fragile X mental retardation protein in binaural brainstem neurons: a comparative study in the alligator, chicken, gerbil, and human, J. Comp. Neurol. 522 (9) (2014) 2107–2128.
[20] S.L. Johnson, Membrane properties specialize mammalian inner hair cells for frequency or intensity encoding, elife 4 (2015) (pii: e08177).
[21] T.P. Franken, M.T. Roberts, L. Wei, N.L. Golding, P.X. Joris, In vivo coincidence detection in mammalian sound localization generates phase delays, Nat. Neurosci. 18 (3) (2015) 444–452.
[22] T.M. Mowery, V.C. Kotak, D.H. Sanes, The onset of visual experience gates auditory cortex critical periods, Nat. Commun. 7 (2016) 10416.
[23] G. von Trapp, B.N. Buran, K. Sen, M.N. Semple, D.H. Sanes, A decline in response variability improves neural signal detection during auditory task performance, J. Neurosci. 36 (43) (2016) 11097–11106.
[24] S.L. Johnson, J. Olt, S. Cho, H. von Gersdorff, W. Marcotti, The coupling between Ca2+ channels and the exocytotic Ca2+ sensor at hair cell ribbon synapses varies tonotopically along the mature cochlea, J. Neurosci. 37 (9) (2017) 2471–2484.
[25] A. Stange-Marten, A.L. Nabel, J.L. Sinclair, M. Fischl, O. Alexandrova, H. Wohlfrom, C. Kopp-Scheinpflug, M. Pecka, B. Grothe, Input timing for spatial processing is precisely tuned via constant synaptic delays and myelination patterns in the auditory brainstem, Proc. Natl. Acad. Sci. U. S. A. 114 (24) (2017) E4851–E4858.
[26] J.J. Rosowski, M.E. Ravicz, S.W. Teoh, D. Flandermeyer, Measurements of middle-ear function in the Mongolian gerbil, a specialized mammalian ear, Audiol. Neurootol. 4 (3–4) (1999) 129–136.
[27] W.X. Chan, S.H. Lee, N. Kim, C.S. Shin, Y.J. Yoon, Mechanical model of an arched basilar membrane in the gerbil cochlea, Hear. Res. 345 (2017) 1–9.
[28] M. Risoud, J. Sircoglou, G. Dedieu, M. Tardivel, C. Vincent, N.X. Bonne, Imaging and cell count in cleared intact cochlea in the Mongolian gerbil using laser scanning confocal microscopy, Eur. Ann. Otorhinolaryngol. Head Neck Dis. 134 (4) (2017) 221–224.
[29] B.D. Winters, S.X. Jin, K.R. Ledford, N.L. Golding, Amplitude normalization of dendritic EPSPs at the Soma of binaural coincidence detector neurons of the medial superior olive, J. Neurosci. 37 (12) (2017) 3138–3149.
[30] N.B. Cant, Patterns of convergence in the central nucleus of the inferior colliculus of the Mongolian gerbil: organization of inputs from the superior olivary complex in the low frequency representation, Front. Neural Circuits 6 (7) (2013) 29.
[31] N.B. Cant, C.G. Benson, Organization of the inferior colliculus of the gerbil (Meriones unguiculatus): differences in distribution of projections from the cochlear nuclei and the superior olivary complex, J. Comp. Neurol. 495 (5) (2006) 511–528.
[32] N.B. Cant, C.G. Benson, Multiple topographically organized projections connect the central nucleus of the inferior colliculus to the ventral division of the medial geniculate nucleus in the gerbil, Meriones unguiculatus, J. Comp. Neurol. 503 (3) (2007) 432–453.
[33] N.B. Cant, C.G. Benson, Organization of the inferior colliculus of the gerbil (Meriones unguiculatus): projections from the cochlear nucleus, Neuroscience 154 (1) (2008) 206–217.
[34] S.D. Holman, W.T. Seale, Ontogeny of sexually dimorphic ultrasonic vocalizations in Mongolian gerbils, Dev. Psychobiol. 24 (2) (1991) 103–115.
[35] K.I. Kobayasi, H. Riquimaroux, Classification of vocalizations in the Mongolian gerbil, Meriones unguiculatus, J. Acoust. Soc. Am. 131 (2) (2012) 1622–1631.
[36] M. Ter-Mikaelian, W.B. Yapa, R. Rubsamen, Vocal behavior of the Mongolian gerbil in a seminatural enclosure, Behaviour 149 (2012) 461–492.
[37] L.I. Hellstrom, R.A. Schmiedt, Measures of tuning and suppression in single- fiber and whole-nerve responses in young and quiet-aged gerbils, J. Acoust. Soc. Am. 100 (5) (1996) 3275–3285.
[38] I. Hamann, O. Gleich, G.M. Klump, M.C. Kittel, F.A. Boettcher, R.A. Schmiedt, J. Strutz, Behavioral and evoked-potential thresholds in young and old Mongolian gerbils (Meriones unguiculatus), Hear. Res. 171 (1–2) (2002) 82–95.
[39] W.J. Loskota, P. Lomax, S.T. Rich, The gerbil as a model for the study of the epilepsies. Seizure patterns and ontogenesis, Epilepsia 15 (1974) 109–119.
[40] N. Ludvig, P.A. Farias, C.E. Ribak, An analysis of various environmental and specific sensory stimuli on the seizure activity of the Mongolian gerbil, Epilepsy Res. 8 (1) (1991) 30–35.
[41] T.C. Kang, S.K. Park, J.H. Bahn, S.G. Jeon, S.M. Jo, S.W. Cho, S.Y. Choi, M.H. Won, The alteration of gamma-aminobutyric acid-transaminase expression in the gerbil hippocampus induced by seizure, Neurochem. Int. 38 (7) (2001) 609–614.
[42] I.K. Hwang, S.K. Park, S.J. An, K.Y. Yoo, D.S. Kim, J.Y. Jung, M.H. Won, S.Y. Choi, O.S. Kwon, T.C. Kang, GABAA, not GABAB, receptor shows subunit- and spatial-specific alterations in the hippocampus of seizure prone gerbils, Brain Res. 1003 (1–2) (2004) 98–107.
[43] S.E. Kwak, J.E. Kim, D.S. Kim, J.Y. Jung, M.H. Won, O.S. Kwon, S.Y. Choi, T.C. Kang, Effects of GABAergic transmissions on the immunoreactivities of

calcium binding proteins in the gerbil hippocampus, J. Comp. Neurol. 485 (2) (2005) 153–164.

[44] S. Levine, H. Payan, Effects of ischemia and other procedures on the brain and retina of the gerbil (*Meriones unguiculatus*), Exp. Neurol. 16 (1966) 255–262.

[45] G. Delbarre, B. Delbarre, Y. Barrau, A suitable method to select gerbils with incomplete circle of Willis, Stroke 19 (1) (1988) 126.

[46] G.P. Pelliccioli, C. Gambelunghe, P.F. Ottaviano, S. Iannaccone, M.V. Ambrosini, Variable response of the Mongolian gerbil to unilateral carotid occlusion: magnetic resonance imaging and neuropathological characterization, Ital. J. Neurol. Sci. 16 (8) (1995) 517–526.

[47] D.L. Small, A.M. Buchan, Animal models, Br. Med. Bull. 56 (2) (2000) 307–317.

[48] B.H. Lim, R. Noordin, Z.M. Nor, R.A. Rahman, K.A. Abdullah, S. Sinnadurai, *Brugia malayi* infection in *Meriones unguiculatus*: antibody response to recombinant BmR1, Exp. Parasitol. 108 (1–2) (2004) 1–6.

[49] S. Shigeno, Y. Fujimaki, K. Toriyama, A. Ichinose, Y. Mitsui, Y. Aoki, E. Kimura, Temporary shift of microfilariae of *Brugia pahangi* from the lungs to muscles in Mongolian jirds, *Meriones unguiculatus*, after a single injection of diethylcarbamazine, J. Parasitol. 92 (5) (2006) 1075–1080.

[50] M.P. Hübner, M.N. Torrero, J.W. McCall, E. Mitre, *Litomosoides sigmodontis*: a simple method to infect mice with L3 larvae obtained from the pleural space of recently infected jirds (*Meriones unguiculatus*), Exp. Parasitol. 123 (1) (2006) 95–98.

[51] R.M. Peek, Helicobacter pylori infection and disease: from humans to animal models, Dis. Model. Mech. 1 (1) (2008) 50–55.

[52] A.H. Wences, M.C. Schatz, Metassembler: merging and optimizing de novo genome assemblies, Genome Biol. 16 (2008) 207.

[53] M. Boetzer, C.V. Henkel, H.J. Jansen, D. Butler, W. Pirovano, Scaffolding pre-assembled contigs using SSPACE, Bioinformatics 27 (4) (2011) 578–579.

[54] A.F.A. Smit, R. Hubley, RepeatModeler Open-1.0, http://www.repeatmasker.org, (2008–2015).

[55] NCBI Eukaryotic genome annotation pipeline guidelines https://www.ncbi.nlm.nih.gov/genome/annotation_euk/process/.

[56] C. Soderlund, W. Nelson, A. Shoemaker, A. Paterson, SyMAP: a system for discovering and viewing syntenic regions of FPC maps, Genome Res. 16 (9) (2006) 1159–1168.

[57] TriFusion v0.5.0 pipeline http://odiogosilva.github.io/TriFusion/.

[58] S. Fischer, B.P. Brunk, F. Chen, X. Gao, O.S. Harb, J.B. Iodice, D. Shanmugam, D.S. Roos, C.J. Stoeckert Jr., Using OrthoMCL to assign proteins to OrthoMCL-DB groups or to cluster proteomes into new ortholog groups, Curr. Protoc. Bioinformatics 35 (6.12) (2011) 6.12-1–6.12-19 (Chapter 6).

[59] D.W. Huang, B.T. Sherman, R.A. Lempicki, Systematic and integrative analysis of large gene lists using DAVID bioinformatics resources, Nat. Protoc. 4 (2009) 44–57.

[60] F.A. Simão, R.M. Waterhouse, P. Ioannidis, E.V. Kriventseva, E.M. Zdobnov, BUSCO: assessing genome assembly and annotation completeness with single-copy orthologs, Bioinformatics 31 (19) (2015) 3210–3212.

[61] E.B. Kim, S.G. Lee, The complete mitochondrial genome of the Mongolian gerbil, *Meriones unguiculatus* (Rodentia: Muridae: Gerbillinae), Mitochondrial DNA A DNA Mapp. Seq. Anal 27 (2016) 1457–1458.

[62] C.L. Li, X.Y. Du, J. Gao, C. Wang, H.G. Guo, F.W. Dai, X.Y. Sa, W. An, Z.W. Chen, Phylogenetic analysis of the Mongolian gerbil (*Meriones unguiculatus*) from China based on mitochondrial genome, Genet. Mol. Res. 15 (3) (2016).

[63] T.S. Painter, A comparison of the chromosomes of the rat and mouse with reference to the question of chromosome homology in mammals, Genetics 13 (1928) 181–189.

[64] M.A. Biscotti, E. Olmo, J.S. Heslop-Harrison, Repetitive DNA in eukaryotic genomes, Chromosom. Res. 23 (3) (2015) 415–420.

[65] Y. Mostovoy, M. Levy-Sakin, J. Lam, E.T. Lam, A.R. Hastie, P. Marks, J. Lee, C. Chu, C. Lin, Ž. Džakula, H. Cao, S.A. Schlebusch, K. Giorda, M. Schnall-Levin, J.D. Wall, P.Y. Kwok, A hybrid approach for de novo human genome sequence assembly and phasing, Nat. Methods 13 (7) (2016) 587–590.

[66] C. Ratomponirina, E. Viegas-Péquignot, B. Dutrillaux, F. Petter, Y. Rumpler, Synaptonemal complexes in Gerbillidae: probable role of intercalated heterochromatin in gonosome-autosome translocations, Cytogenet. Cell Genet. 43 (3–4) (1986) 161–167.

[67] E. Viegas-Péquignot, T. Benazzou, B. Dutrillaux, F. Petter, Complex evolution of sex chromosomes in Gerbillidae (Rodentia), Cytogenet. Cell Genet. 34 (1–2) (1982) 158–167.

[68] J. Wahrman, C. Richler, E. Neufeld, A. Friedmann, The origin of multiple sex chromosomes in the gerbil *Gerbillus gerbillus* (Rodentia: Gerbillinae), Cytogenet. Cell Genet. 35 (3) (1983) 161–180.

[69] R. de la Fuente, M.T. Parra, A. Viera, A. Calvente, R. Gómez, J.A. Suja, J.S. Rufas, J. Page, Meiotic pairing and segregation of achiasmate sex chromosomes in eutherian mammals: the role of SYCP3 protein, PLoS Genet. 3 (11) (2007) e198.

[70] C. Camacho, G. Coulouris, V. Avagyan, N. Ma, J. Papadopoulos, K. Bealer, T.L. Madden, BLAST +: architecture and applications, BMC Bioinformatics 10 (2008) 421.

[71] B. Kiryutin, A. Souvorov, T. Tatusova, ProSplign - Protein to Genomic Alignment Tool, https://www.ncbi.nlm.nih.gov/sutils/static/prosplign/prosplign.html.

[72] E. Carafoli, Intracellular calcium homeostasis, Annu. Rev. Biochem. 56 (1987) 395–433.

[73] S.A. Thayer, Y.M. Usachev, W.J. Pottorf, Modulating Ca2+ clearance from neurons, Front. Biosci. 1 (7) (2002) (d1255-79).

[74] J.G. Duman, L. Chen, B. Hille, Calcium transport mechanisms of PC12 cells, J. Gen. Physiol. 2131 (4) (2008) 307–323.

[75] R.A. Dumont, U. Lins, A.G. Filoteo, J.T. Penniston, B. Kachar, P.G. Gillespie,

[76] P.J. Kozel, R.A. Friedman, L.C. Erway, E.N. Yamoah, L.H. Liu, T. Riddle, J.J. Duffy, T. Doetschman, M.L. Miller, E.L. Cardell, G.E. Shull, Balance and hearing deficits in mice with a null mutation in the gene encoding plasma membrane Ca2+-ATPase isoform 2, J. Biol. Chem. 273 (30) (1998) 18693–18696.

[77] P.J. Kozel, R.R. Davis, E.F. Krieg, G.E. Shull, L.C. Erway, Deficiency in plasma membrane calcium ATPase isoform 2 increases susceptibility to noise-induced hearing loss in mice, Hear. Res. 164 (1–2) (2002) 231–239.

[78] V.A. Street, J.W. McKee-Johnson, R.C. Fonseca, B.L. Tempel, K. Noben-Trauth, Mutations in a plasma membrane Ca2+-ATPase gene cause deafness in deaf-waddler mice, Nat. Genet. 19 (4) (1998) 390–394.

[79] A.R. Penheiter, A.G. Filoteo, C.L. Croy, J.T. Penniston, Characterization of the deafwaddler mutant of the rat plasma membrane calcium-ATPase2 2, Hear. Res. 62 (1–2) (2001) 19–28.

[80] J.M. Schultz, Y. Yang, A.J. Caride, A.G. Filoteo, A.R. Penheiter, A. Lagziel, R.J. Morell, S.A. Mohiddin, L. Fananapazir, A.C. Madeo, J.T. Penniston, A.J. Griffith, Modification of human hearing loss by plasma-membrane calcium pump PMCA2, N. Engl. J. Med. 352 (15) (2005) 1557–1564.

[81] M. Brini, F. Di Leva, T. Domi, L. Fedrizzi, D. Lim, E. Carafoli, Plasma-membrane calcium pumps and hereditary deafness, Biochem. Soc. Trans. 35 (2007) 913–918.

[82] B.L. Tempel, D.J. Shilling, The plasma membrane calcium ATPase and disease, Subcell. Biochem. 45 (2007) 365–383.

[83] Y. Wang, D.E. Cunningham, B.L. Tempel, E.W. Rubel, Compartment-specific regulation of plasma membrane calcium ATPase type 2 in the chick auditory brainstem, J. Comp. Neurol. 514 (6) (2009) 624–640.

[84] J.H. Weatherstone, C. Kopp-Scheinpflug, N. Pilati, Y. Wang, I.D. Forsythe, E.W. Rubel, B.L. Tempel, Maintenance of neuronal size gradient in MNTB requires sound-evoked activity, J. Neurophysiol. 117 (2) (2017) 756–766.

[85] S. Srivastava, J. Cohen, J. Pevsner, S. Aradhya, D. McKnight, E. Butler, M. Johnston, A. Fatemi, A novel variant in GABRB2 associated with intellectual disability and epilepsy, Am. J. Med. Genet. A 164A (11) (2014) 2914–2921.

[86] H. Kodera, C. Ohba, M. Kato, T. Maeda, K. Araki, D. Tajima, M. Matsuo, N. Hino-Fukuyo, K. Kohashi, A. Ishiyama, S. Takeshita, H. Motoi, T. Kitamura, A. Kikuchi, Y. Tsurusaki, N. Nakashima, N. Miyake, M. Sasaki, S. Kure, K. Haginoya, H. Saitsu, N. Matsumoto, De novo GABRA1 mutations in Ohtahara and West syndromes, Epilepsia 57 (4) (2016) 566–573.

[87] M.P. Gontika, C. Konialis, C. Pangalos, A. Papavasiliou, Novel SCN1A and GABRA1 gene mutations with diverse phenotypic features and the question on the existence of a broader spectrum of Dravet syndrome, Child Neurol. Open 4 (2017) (2329048X17706794).

[88] G. Choii, J. Ko, Gephyrin: a central GABAergic synapse organizer, Exp. Mol. Med. 47 (2015) e158.

[89] L. Gan, L.K. Kaczmarek, When, where, and how much? Expression of the Kv3.1 potassium channel in high-frequency firing neurons, J. Neurobiol. 37 (1) (1998) 69–79.

[90] B. Rudy, C.J. McBain, Kv3 channels: voltage-gated K+ channels designed for high-frequency repetitive firing, Trends Neurosci. 24 (9) (2001) 517–526.

[91] P.J. Mathews, P.E. Jercog, J. Rinzel, L.L. Scott, N.L. Golding, Control of sub-millisecond synaptic timing in binaural coincidence detectors by K(v)1 channels, Nat. Neurosci. 13 (5) (2010) 601–609.

[92] R.J. Hagerman, E. Berry-Kravis, W.E. Kaufmann, M.Y. Ono, N. Tartaglia, A. Lachiewicz, R. Kronk, C. Delahunty, D. Hessl, J. Visootsak, J. Picker, L. Gane, M. Tranfaglia, Advances in the treatment of fragile X syndrome, Pediatrics 123 (1) (2009) 378–390.

[93] M. Raspa, A.C. Wheeler, C. Riley, Public health literature review of fragile X syndrome, Pediatrics 139 (Suppl. 3) (2017) S153–S171.

[94] K. Beebe, Y. Wang, R. Kulesza, Distribution of fragile X mental retardation protein in the human auditory brainstem, Neuroscience 273 (2014) 79–91.

[95] R.J. Kulesza Jr., R. Lukose, L.V. Stevens, Malformation of the human superior olive in autistic spectrum disorders, Brain Res. 1367 (2011) 360–371.

[96] R.J. Kulesza, K. Mangunay, Morphological features of the medial superior olive in autism, Brain Res. 1200 (2008) 132–137.

[97] R. Lukose, K. Beebe, R.J. Kulesza Jr., Organization of the human superior olivary complex in 15q duplication syndromes and autism spectrum disorders, Neuroscience 286 (2015) 216–230.

[98] P.M. Rodier, J.L. Ingram, B. Tisdale, S. Nelson, J. Romano, Embryological origin for autism: developmental anomalies of the cranial nerve motor nuclei, J. Comp. Neurol. 370 (2) (1996) 247–261.

[99] Y. Wang, H. Sakano, K. Beebe, M.R. Brown, R. de Laat, M. Bothwell, R.J. Kulesza Jr., E.W. Rubel, Intense and specialized dendritic localization of the fragile X mental retardation protein in binaural brainstem neurons: a comparative study in the alligator, chicken, gerbil, and human, J. Comp. Neurol. 522 (9) (2014) 2107–2128.

[100] G. Gimpl, F. Fahrenholz, The oxytocin receptor system: structure, function, and regulation, Physiol. Rev. 81 (2) (2001) 629–683.

[101] Caldwell H, Young W. (2006). Oxytocin and vasopressin: genetics and behavioral implications. In *Structure*, Ed R. Lim (New York, NY: Springer), 573–607.

[102] A. Kiss, J.D. Mikkelsen, Oxytocin—anatomy and functional assignments: a mini-review, Endocr. Regul. 39 (3) (2005) 97–105.

[103] A.H. Veenema, I.D. Neumann, Central vasopressin and oxytocin release: regulation of complex social behaviours, Prog. Brain Res. 170 (2008) 261–276.

[104] R.L. Pobbe, B.L. Pearson, E.B. Defensor, V.J. Bolivar, W.S. Young 3rd, H.J. Lee, D.C. Blanchard, R.J. Blanchard, Oxytocin receptor knockout mice display deficits in the expression of autism-related behaviors, Horm. Behav. 61 (3) (2012) 436–444.